Modeling of Char Oxidation in Fluidized Bed Biomass Gasifiers: Effects of Transport and Chemical Kinetics

by

Amelia Brooks

Submitted to the
Department of Mechanical Engineering
in Partial Fulfillment of the Requirements for the Degree of

Bachelor of Science in Mechanical Engineering

at the

Massachusetts Institute of Technology

June 2015

Signature redacted

Signature of Author: _____
Department of Mechanical Engineering
May 21, 2015

Signature redacted

Certified by: _____
Ahmed F. Ghoniem
Ronald C. Crane (1972) Professor
Director, Center for Energy and Propulsion Research
Director, Reacting Gas Dynamics Laboratory
Thesis Supervisor

Signature redacted

Accepted by: _____
Anette Hosoi
Professor of Mechanical Engineering
Undergraduate Officer

Modeling of Char Oxidation in Fluidized Bed Biomass Gasifiers: Effects of Transport and Chemical Kinetics

by

Amelia Brooks

Submitted to the Department of Mechanical Engineering on May 21, 2015
in Partial Fulfillment of the Requirements for the Degree of
Bachelor of Science in Mechanical Engineering

ABSTRACT

Technologies for the conversion of biomass to liquid fuels are important to develop because the demand for liquid fuels remains unchanged even with the necessity of limiting dependence on fossil fuels. Fluidized Bed Biomass Gasification (FBBG) is one such technology that can perform the initial step of converting raw biomass into syngas as an intermediate to liquid fuels. The char that is left in the reactor after devolatilization can be oxidized in order to maximize the amount of biomass carbon that is converted to gaseous carbon and generate heat to drive endothermic gasification reactions. This paper examines the rate of each of the three processes that occur during char conversion (external diffusion, chemical reactions, and intraparticle diffusion) to determine which process limits the rate of the reaction under a range of conditions. It was determined that at most FBBG operating points, the rate of char conversion will be limited by the rate of diffusion of oxygen through the particle's boundary layer and through its pores. Only at low reactor temperatures and small particle diameters will the reaction rate be purely kinetically limited. An overall rate expression accounting for all three processes has been formulated which can be implemented in more detailed reactor models.

Thesis Supervisor: Ahmed Ghoniem

Title: Ronald C. Crane (1972) Professor; Director, Center for Energy and Propulsion Research; Director, Reacting Gas Dynamics Laboratory

Acknowledgments

I would like to thank Professor Ahmed Ghoniem, Richard Bates, and Dr. Christos Altantzis for their guidance, feedback, and support over the course of this project.

Table of Contents

1. Introduction **7**

1.1 Biomass as a fuel source 7

1.2 Biomass Gasification 7

1.2.1 Biomass Conversion in a Fluidized Bed Biomass Gasifier (FBBG) 7

1.3 Char Conversion 8

1.2.1 External Mass Transfer 10

1.2.2 Chemical Reactions 10

1.2.3 Internal Mass Transfer 10

2. Methodology and Mathematical Models **11**

2.1 Model Overview and Assumptions 11

2.2 Rate of External Mass Transfer 11

2.2.1 Comparison of Correlations for Mass Diffusivity 12

2.2.2 Comparison of Correlations for Sherwood Number 14

2.2.3 Computation of Mass Transfer Coefficient and Burnout Time for External Mass Transfer 17

2.3 Rate of Chemical Reactions 19

2.3.1 Comparisons of Oxidation Reaction Rate Expressions 19

2.3.1 Comparison of Burnout Times Under Various Reactor Conditions 20

2.4 Rate of Internal Mass Transfer 22

2.4.1 Overview 22

2.4.2 Governing Equations and Parameters 22

2.4.3 Burnout Time for Internal Diffusion-Limited Conditions 27

2.5 Overall Char Oxidation Process 28

2.5.1 Char Oxidation Rate 28

2.5.2 Char Oxidation Burnout Time 29

2.6 Conditions Under Which Mass Transfer is Limiting 30

3. Results **30**

3.1 Reaction Rate as a Function of Temperature 30

3.2 Mass Transfer Limitation Threshold 34

4. Conclusion **35**

5. References **36**

1. Introduction

1.1 Biomass as a fuel source

Biomass provides a renewable alternative to fossil-derived fuels and is an important fuel source to develop in the face of global warming and rising oil prices. Many conversion pathways have been developed for the production of liquid fuels and other chemicals from biomass, several of which are developed enough to be used commercially. With the growing necessity of reducing dependence on oil and no change in demand for liquid fuels, it is becoming more important to improve on existing biomass-based fuel technologies.

1.2 Biomass Gasification

1.2.1 Biomass Conversion in a Fluidized Bed Biomass Gasifier (FBBG)

The Fluidized Bed Biomass Gasifier (FBBG) is the reactor studied in this paper. In a FBBG, raw biomass is fed into a bed of a material of high thermal inertia (often sand) at a temperature of 700-1000°C. The bed is subject to a high velocity air stream to ensure uniform conversion of solid biomass to syngas throughout the reactor.

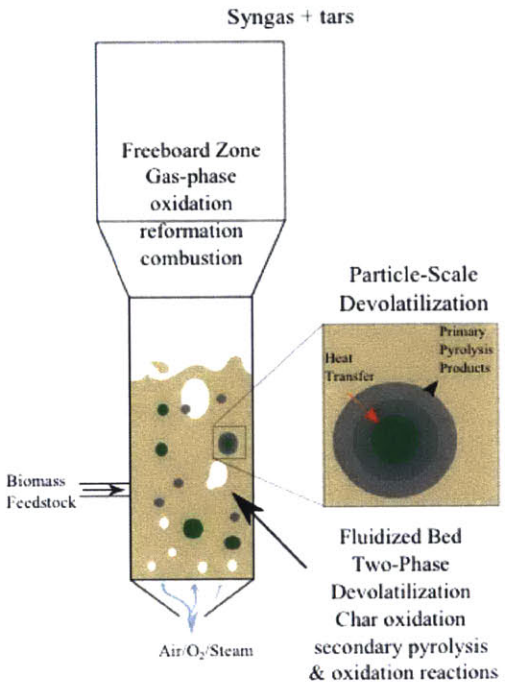

Figure 1: Schematic of a Fluidized Bed Biomass Gasifier (FBBG). Raw biomass is fed into a bed of sand which is fluidized by a stream of air below, and reacts to form syngas [1].

During the conversion process, raw biomass will undergo devolatilization in the presence of oxygen, producing char and a mixture of hydrocarbons. The majority of the resulting char will be gasified, yielding a product that is a mixture of syngas (hydrogen and carbon dioxide) and perfect combustion products (water and carbon dioxide). Syngas, the desired product, then undergoes the Fischer-Tropsch catalytic process to convert it to diesel range liquid fuels. However, a nonnegligible portion of the biomass will be left in the reactor as solid char, which is essentially pure carbon. The remaining char is oxidized, converting some to carbon monoxide and some to carbon dioxide. Since the desired output of the gasification process is syngas, the efficiency of the process can be improved by maximizing the amount of biomass carbon that is converted to gaseous carbon rather than left in the reactor as solid carbon.

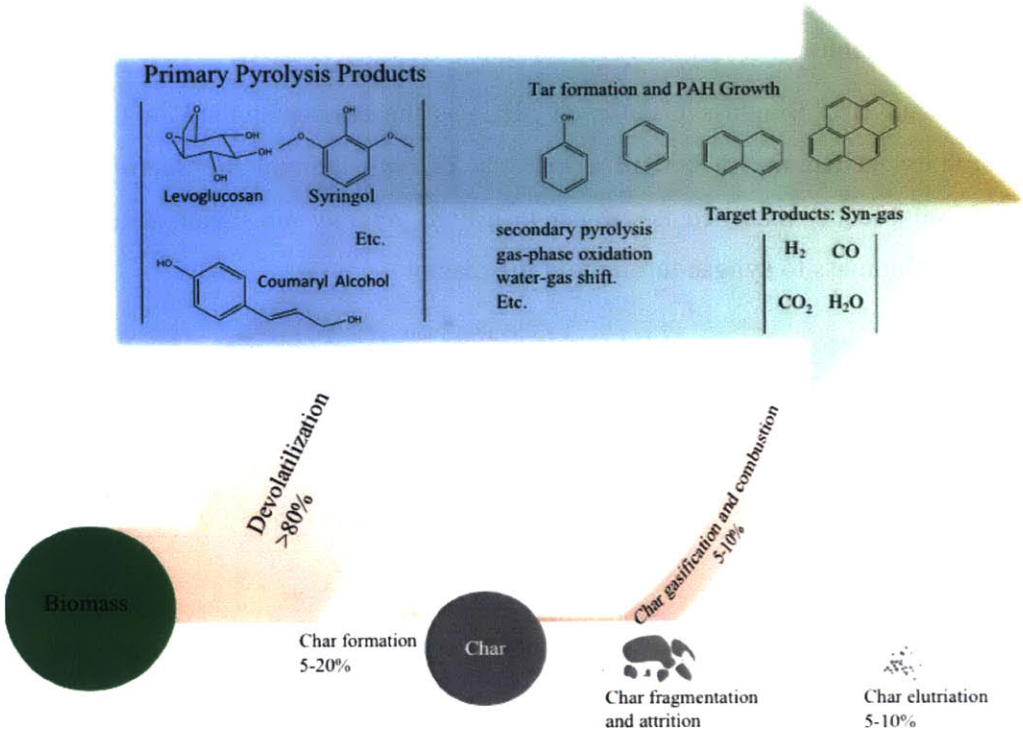

Figure 2: The processes occurring inside a fluidized bed gasifier. This paper focuses on the char gasification and combustion step [1].

1.3 Char Conversion

During char oxidation, oxygen diffuses through the char particle's boundary layer and reacts with solid carbon at the particle's surface and inside its pores to produce carbon monoxide and carbon dioxide. There are three physical and chemical processes that occur during this

reaction: external diffusion, internal diffusion, and chemical reactions. The overall char conversion rate will be determined by the rate of each process and will be limited by the slowest one. Each process and its limitations will be discussed in detail in this section.

The three limiting cases are pictured in Figure 3. In Zone I, chemical reactions inside the particle are the slowest of the three processes, meaning oxygen can diffuse through the particle's boundary layer and pores much faster than it is consumed. In Zone II, internal mass transfer is the limiting process, and chemical reactions occur comparatively fast enough that a concentration gradient forms across the particle radius. In Zone III, external mass transfer is the slowest process, so that a concentration gradient will form in the particle's boundary layer because the rate of external mass transfer cannot keep up with the rate at which oxygen is being consumed in the particle.

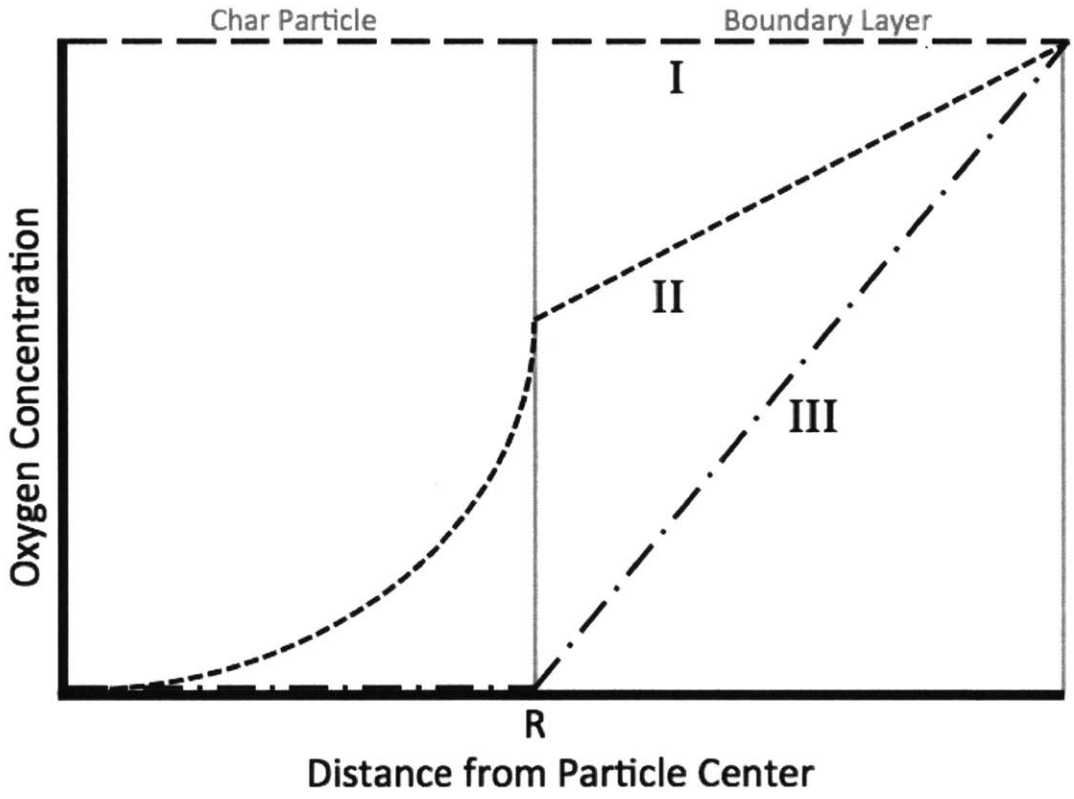

Figure 3: Oxygen concentration as a function of the distance from the center of the char particle. Zone I: chemical reactions are slow. Zone II: internal mass transfer is slow. Zone III: external mass transfer is slow.

1.3.1 External Mass Transfer

For char oxidation in a FBBG, external mass transfer refers to the diffusion of oxygen through the boundary layer of a char particle. External diffusion is most commonly characterized by several parameters, including mass diffusivity, the dimensionless Sherwood number, and mass transfer coefficient. Several correlations for diffusivity and Sherwood number are presented and compared in section 2.1, but the mass transfer coefficient is a constant that can be given by

$$h_m = \frac{J}{\Delta c_A} = \frac{Sh \cdot D_g}{L} \quad \left[\frac{\text{m}}{\text{s}}\right] \tag{1}$$

where

$\dot{n}_A$= mass transfer rate $\left[\frac{\text{mol}}{\text{s}}\right]$

J = molar flux, $\left[\frac{\text{mol}}{\text{m}^2 \cdot \text{s}}\right]$

A = surface area over which mass transfer occurs [m^2]

Δc_A= concentration difference driving the mass transfer $\left[\frac{\text{mol}}{\text{m}^3}\right]$

Sh = Sherwood number [dimensionless]

D_g = mass diffusivity $\left[\frac{\text{m}^2}{\text{s}}\right]$

L = characteristic length scale [m]

An oxidation process limited by external mass transfer would be characterized by an oxygen concentration gradient outside the char particle, with no oxygen inside the particle.

1.3.2 Chemical Reactions

Once raw biomass has been devolatilized, the char particles remaining in the FBBG are oxidized by the following reaction:

$$\text{C} + \lambda\text{O}_2 \rightarrow (2 - 2\lambda)\text{CO} + (2\lambda - 1)\text{CO}_2 \tag{2}$$

Since oxygen reacts with the carbonaceous surfaces of the pore walls, the oxidation reaction rate will depend on the surface area of the particle. Since the particle is shrinking as oxygen is consumed, surface area will decrease as the reaction proceeds.

1.3.3 Internal Mass Transfer

Internal mass transfer refers to the diffusion of oxygen across a concentration gradient inside a porous char particle. The rate of internal diffusion is related to the rate of external mass transfer under those conditions but scaled by a factor accounting for limitations due to the

particle's pore structure. Internal mass transfer is governed by Fick's Law of Diffusion, which relates the mass flux through an area to the concentration of the gaseous specie by

$$J = -D\frac{dC}{dx} \tag{3}$$

where J is mass flux $\left[\frac{\text{mol}}{\text{m}^2 \cdot \text{s}}\right]$, D is mass diffusivity $\left[\frac{\text{m}^2}{\text{s}}\right]$, C is specie concentration $\left[\frac{\text{mol}}{\text{m}^3}\right]$, and x is position [m].

2. Methodology and Mathematical Models

2.1 Model Overview and Assumptions

The overall rate and timescale of char oxidation is a function of the rates and timescales of external mass transfer, internal mass transfer, and chemical kinetics during oxidation. In this section, the rate of each process is analytically determined, and all three are compared to show their relationship to the overall rate and timescale.

The following simplifying assumptions about char oxidation in a FBBG are made for the remainder of the paper:

- Spherical particle geometry
- Quasi-steady-state
- Isothermal and isobaric conditions
- Equimolar counter-diffusion of reactants and products

2.2 Rate of External Mass Transfer

The mass diffusivity of a char particle can be computed as a function of the temperature and pressure in the reactor. Several correlations are used to compute mass diffusivity, and the resulting values are compared to the diffusivity values computed using Cantera, a software tool for computing fluid properties. This comparison is used to select a correlation for mass diffusivity that will be used for the remainder of the paper. Using the best diffusivity correlation, the Sherwood number, the ratio of convective to diffusive mass transport in a particle, is then computed. Several correlations for the Sherwood number are also compared. After selecting the best Sherwood correlation, the mass transfer coefficient is determined by the following relation:

$$h_m = \frac{Sh \cdot D_g}{d_p} \quad \left[\frac{\text{m}}{\text{s}}\right] \tag{4}$$

The mass transfer coefficient can then be plugged into an oxidation rate expression to determine the timescale for external mass transfer limited char oxidation.

2.2.1 Comparisons of correlations for mass diffusivity

In this section, two correlations for mass diffusivity from literature are presented and compared to a comprehensive model of binary diffusivity for a species in a mixture.

GERBER CORRELATION

The Gerber correlation can be used for any binary mixture, but here is used to estimate the mass diffusivity of oxygen in a char combustion rate expression [2]. The correlation gives mass diffusivity as a function of reactor temperature and pressure by the following relation:

$$D_{\text{g,Gerber}} = 3.13 \times 10^{-4} \cdot \frac{p_{\text{atm}}}{p} \cdot \left(\frac{T}{1500}\right)^{1.75} \quad \left[\frac{\text{m}^2}{\text{s}}\right] \tag{5}$$

PERRE CORRELATION

The Perre correlation gives mass diffusivity for water vapor in an air mixture as a function of reactor temperature and pressure in the following relation [3].

$$D_{\text{g,Perre}} = 1.192 \times 10^{-4} \frac{T^{1.75}}{p_{\text{atm}}} \quad \left[\frac{\text{m}^2}{\text{s}}\right] \tag{6}$$

GRI/CANTERA METHOD

Mass diffusivity is also computed using a GRI mechanism that models combustion and computes fluid properties using Cantera. This method is the most accurate means of computing mass diffusivity, and is the basis on which the Gerber and Perre correlations should be compared. The three correlations are plotted in Figure 4 as a function of pressure at 800°C, and in Figure 5 as a function of temperature at 1 atm.

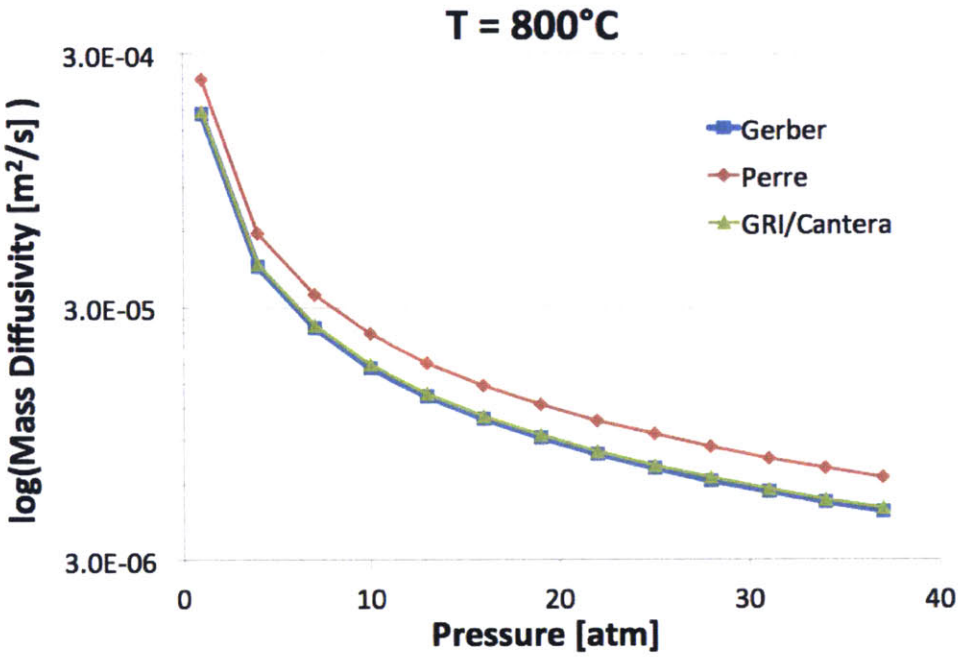

Figure 4: Mass diffusivity as a function of pressure at 800°C from the GRI/Cantera method as well as the Gerber and Perre Correlations.

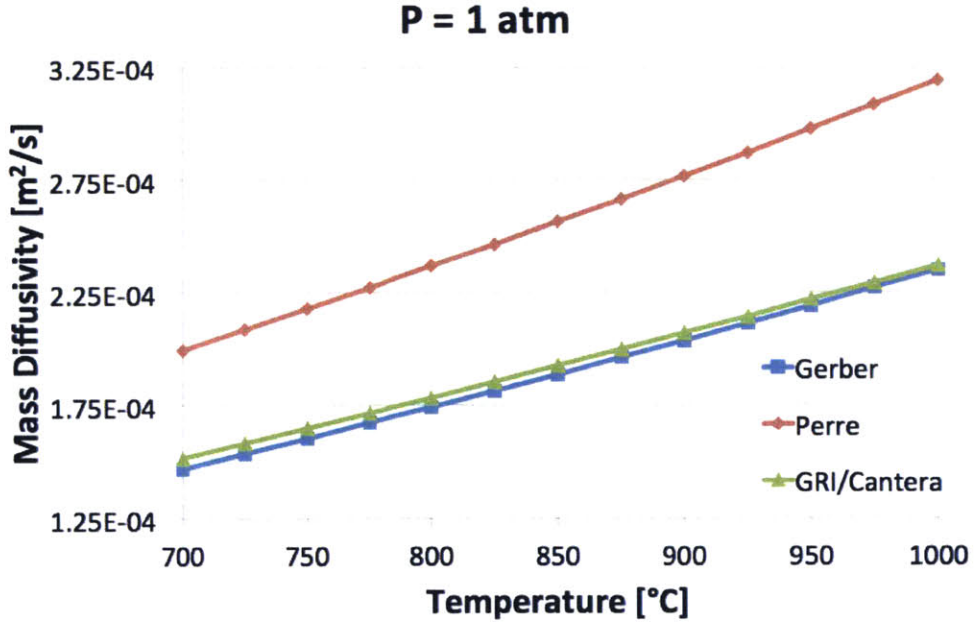

Figure 5: Mass diffusivity as a function of temperature at 1 atm from the GRI/Cantera method as well as the Gerber and Perre Correlations.

The Gerber correlation gives values much closer to the ones computed using the GRI script, and will be the mass diffusivity correlation used for the remainder of the paper.

2.2.2 Comparisons of correlations for Sherwood number

In this section, several correlations from literature are used to compute the Sherwood number, a ratio of convective to diffusive mass transfer in a particle and a means of obtaining its mass transfer coefficient and ultimately the characteristic timescale of external mass transfer-limited char oxidation.

RANZ-MARSHALL

The Ranz-Marshall correlation for Sherwood number is given by

$$Sh = 2 + 0.6\, Re^{\frac{1}{2}}\, Sc^{\frac{1}{3}} \tag{7}$$

and is plotted in Figure 6 as a function of both char particle diameter and char particle velocity. The Reynolds number is a dimensionless number that expresses the ratio of inertial to viscous forces in a fluid flow:

$$Re = \frac{\rho v d}{\mu} \tag{8}$$

and the Schmidt Number is the dimensionless ratio of momentum diffusivity to mass diffusivity:

$$Sc = \frac{\mu}{\rho D_g} \tag{9}$$

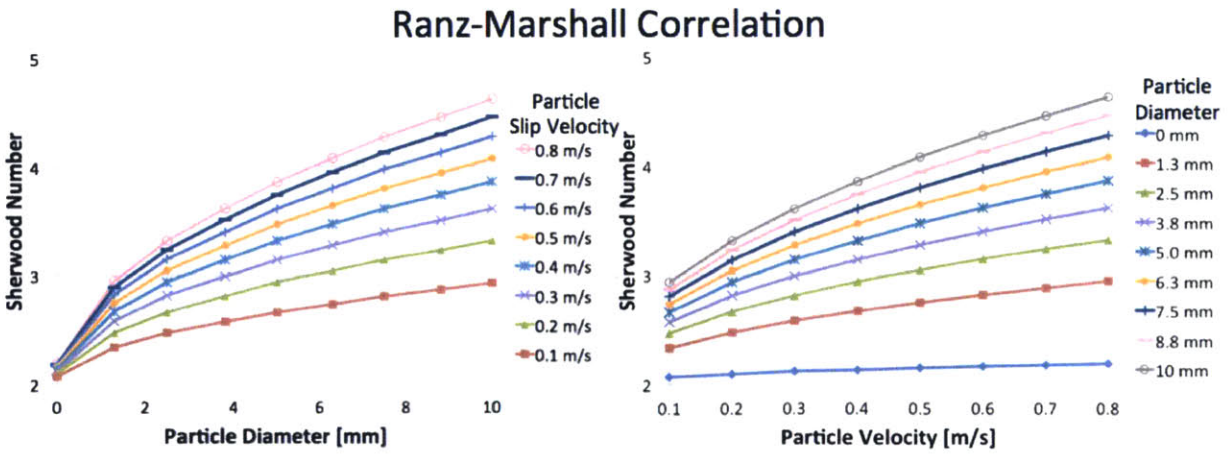

Figure 6: Ranz-Marshall correlation for Sherwood number as a function of char particle velocity and char particle diameter.

The Ranz-Marshall correlation is only valid for Reynolds numbers between 20 and 2000. Reynolds number is shown in Figure 7 as a function of particle diameter and particle velocity. Since the Reynolds number for small particle sizes and velocities does not fall in the valid range, the Ranz-Marshall correlation for Sherwood number is not useful to this model.

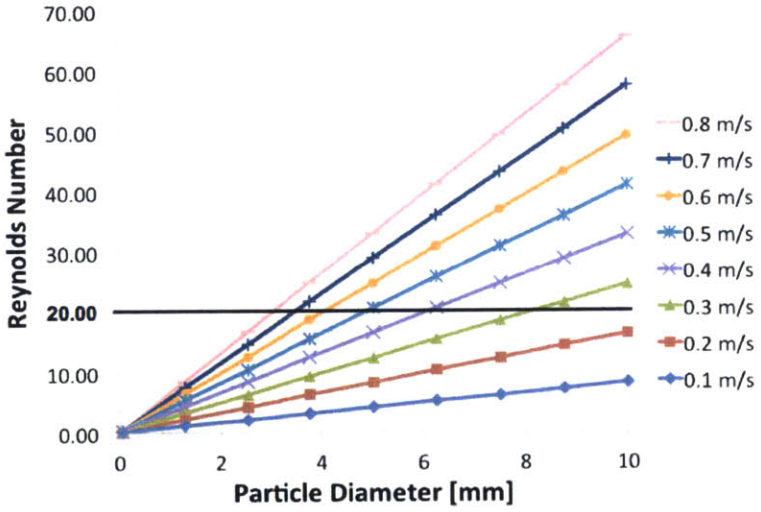

Figure 7: Reynolds number over the range of particle diameters and velocities applicable to char oxidation in a FBBG at 800°C and 1 atm. The point below the black line indicating $Re = 20$ are outside the range for which the Ranz-Marshall correlation is valid.

HAYHURST-PARMAR

The Hayhurst-Parmar correlation for Sherwood number is given by

$$Sh = 2\varepsilon_{\mathrm{mf}} + 0.69\left(\frac{Re_{\mathrm{mf}}}{\varepsilon_{\mathrm{mf}}}\right)^{\frac{1}{2}} Sc^{\frac{1}{3}} \tag{10}$$

Reynolds number is based on the minimum fluidization velocity for sand, which is 0.0438 m/s [4] [5]. $\varepsilon_{\mathrm{mf}}$ is the voidage at minimum fluidization, computed by

$$\varepsilon_{mf} = (14\phi_s)^{-\frac{1}{3}} \tag{11}$$

where ϕ_s is the sphericity of the bed material, which is 0.9 for sand.

PALCHONOK

The Palchonok correlation for Sherwood number is given by

$$Sh = 2\varepsilon_{mf} + 0.177Ar^{0.39}Sc^{\frac{1}{3}} \tag{12}$$

Ar is the Archimedes number, a property of the bed material (sand) that can be computed by the following formula:

$$Ar = \frac{\rho_f g(\rho_p - \rho_f) d_{bp}^3}{\mu_f^2} \tag{13}$$

where ρ_p and ρ_f are the bed particle and gas density, respectively $[\frac{kg}{m^3}]$, d_{bp} is the bed particle diameter [m], and μ_f is the gas viscosity [Pa-s] [6]. In this model, d_{bp} is 0.35 mm and ρ_p is 2600 kg/m^3. This Sherwood correlation is dependent primarily on bed material rather than on char particle geometry and velocity and therefore may not be the best correlation to accurately account for reactor conditions.

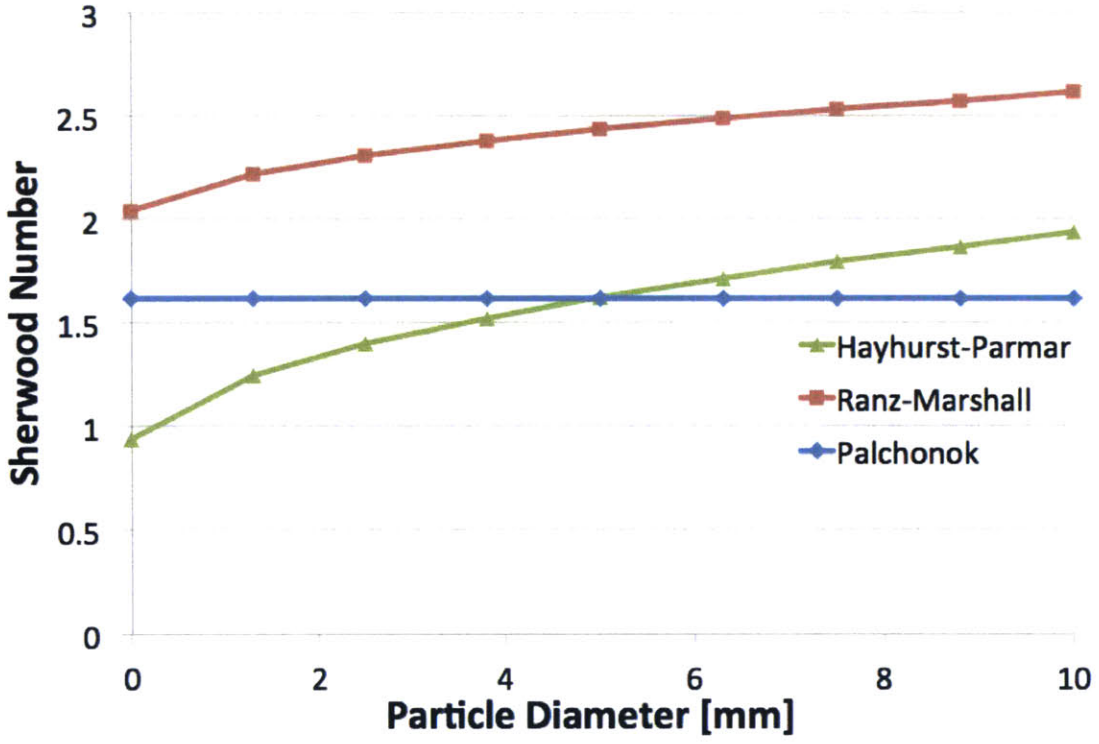

Figure 8: The Hayhurst-Parmar, Ranz-Marshall, and Palchonok correlations for Sherwood number as a function of particle diameter at the minimum fluidization velocity for sand, 0.0438 m/s.

Figure 8 compares these three Sherwood correlations as a function of particle diameter at the minimum fluidization velocity for sand, 0.0438 m/s. Though many correlations for Sherwood number have been developed over the years, it is clear that there is currently no real agreement on Sherwood number for small spherical particles. For the remainder of this paper, the Hayhurst-

Parmar correlation will be used because it is the most recently developed, and the most applicable to the context of this paper.

2.2.3 Computation of Mass Transfer Coefficient and Burnout Time for External Mass Transfer

The mass transfer coefficient is determined by the following equation:

$$h_m = \frac{Sh \cdot D_g}{d_p} \quad \left[\frac{\text{m}}{\text{s}}\right] \tag{14}$$

The Hayhurst-Parmar correlation for Sherwood number was computed at a particle diameter of 5 mm and particle velocity of 0.5 m/s. This value was then plugged into equation **(14)** to yield h_m as a function of temperature and pressure. This dependence is plotted in Figure 9.

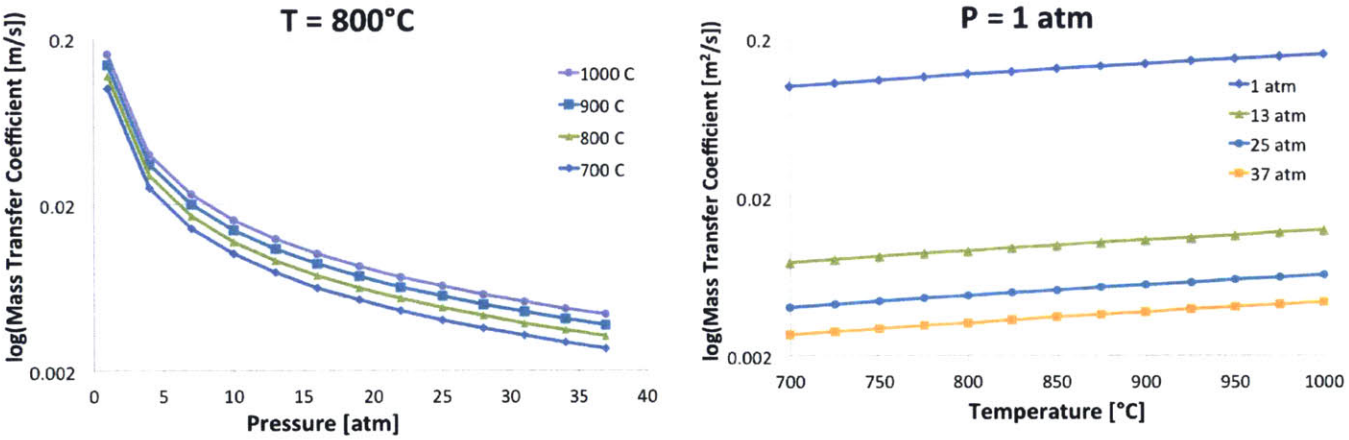

Figure 9: The mass transfer coefficient plotted as function of pressure at 800°C, and as a function of temperature at 1 atm.

The rate of mass transfer of oxygen from the bulk to the particle surface is equal to the particle's surface area times the mass flux to the particle, and is given by the equation

$$r_{O_2} = \pi d_p^2 h_m \{C_{O_2,b} - C_{O_2,s}\} \quad \left[\frac{\text{mol}}{\text{s}}\right] \tag{15}$$

Under the assumption that char oxidation is limited by the rate of external mass transfer and that the reaction kinetics at the surface of the particle are comparatively fast, $C_{O_2,s}$ will approach zero as oxygen is effectively consumed the moment it reaches the particle surface.

The rate of carbon oxidation is also dependent on the oxidation reaction stoichiometry. The distribution of the oxidation products, CO and CO_2, is defined by the following ratio:

$$\eta = \frac{[CO]}{[CO_2]} \tag{16}$$

This can also be expressed as a ratio of the reactants, carbon and O_2, by the following relation:

$$\lambda \left[\frac{\text{mol } O_2}{\text{mol C}}\right] = \frac{1}{2}(1 + \eta \left[\frac{\text{mol CO}}{\text{mol CO+mol } CO_2}\right]) \tag{17}$$

This means that the rate of carbon oxidation (in molC/s) can be expressed as the rate of change of molar mass of the particle

$$r = -\frac{d}{dt}\left(\frac{\pi d_p^3}{6} C_C\right) = \frac{2\pi d_p^2 K_d C_{O_2}}{(1+\eta)} \tag{18}$$

The slope of the plot of d_p^2 versus time will give $Sh/(1 + \eta)$, allowing the Sherwood number to be determined for any point in time [4]. Since the molar density C_C does not change, the oxidation of the char particle will be indicated by a change in particle diameter, allowing the carbon oxidation rate to be expressed as

$$\frac{d(d_p{}^2)}{dt} = -\frac{8ShD_g C_{O_2}}{(1+\eta)C_C} \tag{19}$$

Integrating with respect to time and taking the limit as the particle's diameter goes to zero, the burnout time under external mass transfer limited conditions can now be expressed as

$$t_{\text{b,extMT}} = \frac{d_p^2 C_C \lambda}{4ShD_g C_{O_2}} \tag{20}$$

where $\lambda = \frac{1}{2}(1 + \eta)$. In Figure 10, t_{burnout} is plotted as a function of particle diameter at 1 atm and 800°C, and as a function of reactor temperature for a 5 mm particle at 1atm. Both plots use the minimum fluidization velocity for sand, the bed material, as velocity, and are plotted for three values of λ.

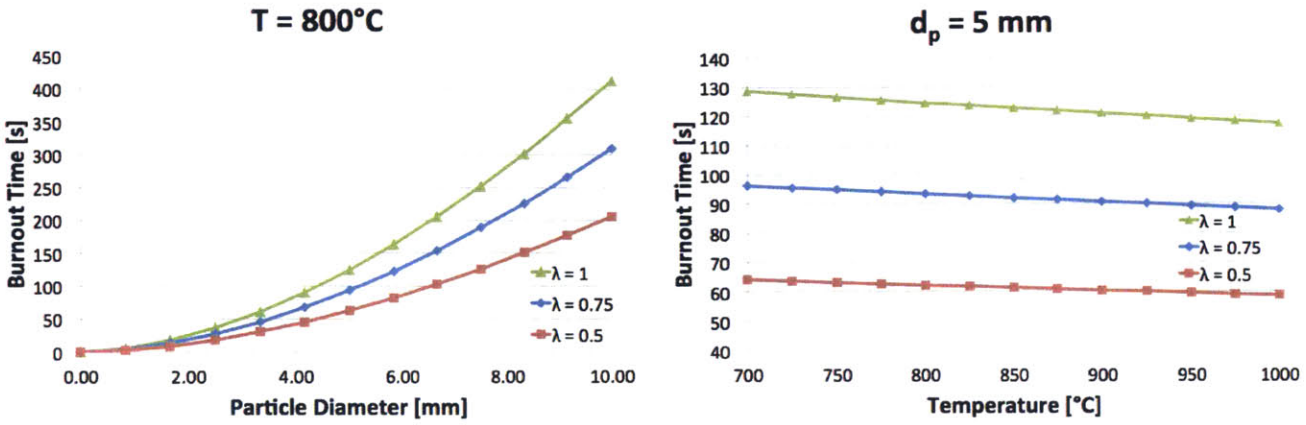

Figure 10: Burnout time as a function of particle diameter at 1 atm and 800°C, and as a function of temperature at 1 atm for a particle with a 5 mm diameter. Burnout time is shown for three values of lambda, which governs the amounts of CO and CO_2 in the products.

Though temperature has a weaker effect on burnout time than particle diameter does, an increase in temperature results in an increase in mass diffusivity that will speed up the overall reaction rate.

2.3 Rate of Chemical Reactions

2.3.1 Comparison of oxidation reaction rate expressions

In this section, two expressions for the rate of char oxidation under kinetically limited conditions are taken from literature and integrated to give a characteristic burnout time for chemical kinetics at the particle surface. These expressions are both written as a function of the char conversion factor, X, which can be expressed as

$$X = \frac{M - M_0}{M_0 - M_\infty} \tag{21}$$

where M_0 and M_∞ are the initial and final mass of the char particle and M is the current mass. X varies from 0 to 1 and is a measure of how much of the original carbon mass in the particle has been oxidized. Burnout time is defined as the time taken to reach $X = 0.99$. The two expressions for burnout time are compared under different reactor conditions as a function of reactor temperature.

DI BLASI RATE EXPRESSION

DiBlasi gives the expression of char oxidation rate as the rate of change of the char conversion factor, X, over time, written as

$$\frac{dX}{dt}\left[\frac{1}{\text{s}}\right] = AP_{O_2}e^{\frac{-E}{RT}}(1-X)^{1.2} \tag{22}$$

where A is a pre-exponential factor equal to 1.5×10^6 $\frac{1}{\text{atm}\cdot\text{s}}$ and E is the activation energy with units of $\frac{\text{kJ}}{\text{mol}}$ [7]. This expression can be rewritten in terms of the molar concentration of oxygen in the reactor, C_{O_2}, as

$$\frac{dX}{dt}\left[\frac{1}{\text{s}}\right] = \frac{ART}{101325}C_{O_2}e^{\frac{-E}{RT}}(1-X)^{1.2} \tag{23}$$

Burnout time for kinetically limited oxidation can be analytically determined by integrating this expression and evaluating X from 0 to 0.99 conversion:

$$t_{\text{burnout}}\,[\text{s}] = \frac{7.5594\cdot101325}{ARTC_{O_2}e^{\frac{-E}{RT}}} \tag{24}$$

In this model, E = 108.74 kJ/mol. The kinetic parameters of the model were all fit for char combustion with air at a heating rate of 10 K/min and a final temperature of 873 K [8].

KASHIWAGI RATE EXPRESSION

Kashiwagi gives char oxidation rate by the following equation:

$$\frac{dX}{dt}\left[\frac{1}{\text{s}}\right] = A\left(\frac{C_{O_2}}{C_{\text{tot}}}\right)^{0.78}e^{\frac{-E}{RT}}(1-X) \tag{25}$$

where, similarly to DiBlasi's rate expression, A is a pre-exponential factor equal to 5.67×10^9 $\frac{1}{\text{atm}^{0.78}\cdot\text{s}}$ and E is the activation energy equal to $160\frac{\text{kJ}}{\text{mol}}$ [9]. Integrating this expression and evaluating X from 0 to 0.99 conversion, burnout time can be written as

$$t_{\text{b,rxn}}\,[s] = \frac{4.6052}{A\left(\frac{C_{O_2}}{C_{\text{tot}}}\right)^{0.78}e^{\frac{-E}{RT}}} \tag{26}$$

2.3.2 Comparison of Burnout Times Under Various Reactor Conditions

In this section, burnout time will be plotted as a function of temperature under different reactor conditions. In Figure 11, burnout time from each rate expression is plotted as a function of temperature under gasification conditions with air of 21% oxygen and 79% nitrogen by volume at atmospheric pressure. In Figure 12, burnout time from each rate expression is plotted as a function of temperature under combustion conditions with air of 4.5% oxygen and 95.5% nitrogen by volume at atmospheric pressure.

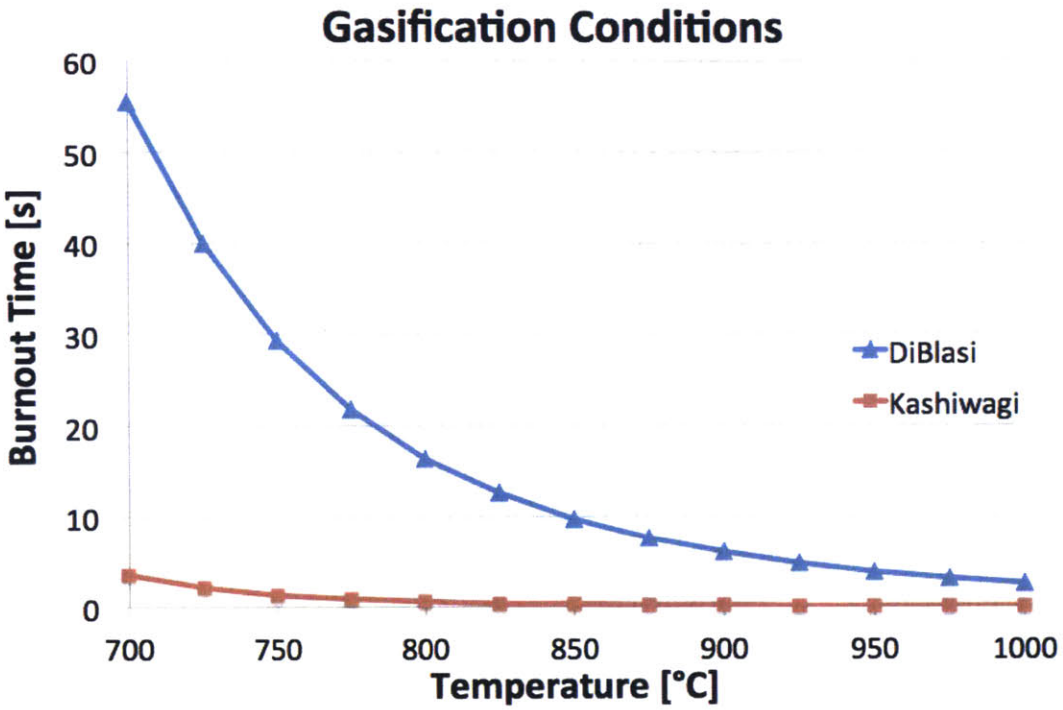

Figure 11: Burnout time vs. temperature under gasification conditions. Air is 4.5% oxygen and 95.5% nitrogen by volume at atmospheric pressure.

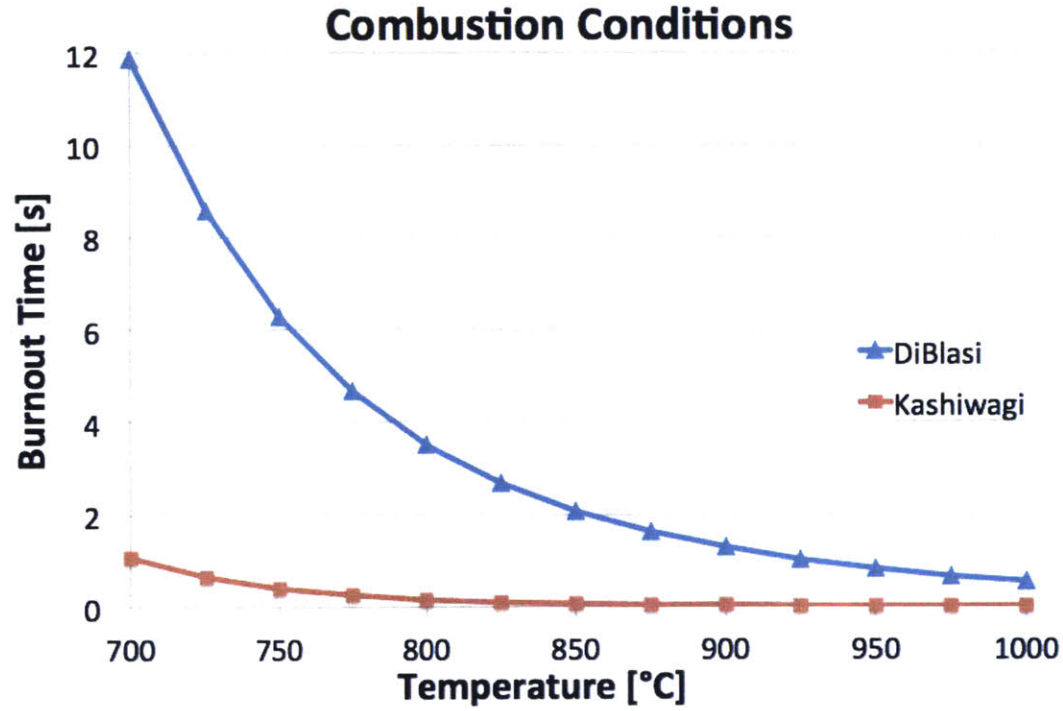

Figure 12: Burnout time vs. temperature under combustion conditions. Air is 21% oxygen and 79% nitrogen by volume at atmospheric pressure.

The Kashiwagi expression for the reaction rate uses a higher activation energy than the DiBlasi expression, indicating a greater temperature dependence for that model. The DiBlasi expression for char oxidation rate is more appropriate for this model since it is fitted for pine wood char, while Kashiwagi's expression is fitted for cellulose, and will be used for the remainder of this paper.

2.4 Rate of Internal Mass Transfer

2.4.1 Overview

The reactant, oxygen, diffuses into the porous char particle. Pores in the particle allow oxygen to diffuse into the particle and react with the carbonaceous surfaces of the pore walls [10]. The overall char internal conversion rate will be a function of parameters related to both internal mass transfer and chemical kinetics.

2.4.2 Governing equation and parameters

The overall char conversion rate, taking into account reaction kinetics and internal and external mass transfer can be given by the steady-state reaction-diffusion governing equation for spherical geometry:

$$\frac{D_{\text{eff}}}{R^2}\frac{d}{dr}\left(R^2\frac{dC_{O_2}}{dr}\right) - kC_{O_2}C_C\lambda = 0 \tag{27}$$

The solution to the governing equation can be written as [11]

$$C_{O_2} = C_s\frac{R}{r}\frac{\sinh(\gamma r)}{\sinh(\gamma R)} \tag{28}$$

and its derivative as

$$\frac{dC_{O_2}}{dr} = C_b\left[\gamma\frac{R}{r}\frac{\cosh(\gamma r)}{\sinh(\gamma R)}\right] \tag{29}$$

where

$$\gamma = \sqrt{\frac{kC_C\lambda}{D_{\text{eff}}}} \tag{30}$$

C_c is the molar density of the char particle, D_{eff} is the effective mass diffusivity, and k is the kinetic rate constant which is equal to

$$k = \frac{ART}{101325}e^{\frac{-E}{RT}} \quad \left[\frac{\text{m}^3}{\text{mol}\cdot\text{s}}\right] \tag{31}$$

from equation (23).

In this section, each parameter of the governing equation is analytically derived for a char particle of spherical geometry undergoing oxidation.

EFFECTIVE DIFFUSIVITY

The mass diffusivity inside a particle must be defined by an effective diffusivity coefficient to account for account for varying diffusion paths and pore structures. This effective diffusion coefficient can be expressed as

$$D_{\text{eff}} = D_g \left(\frac{\varepsilon_g \sigma}{\tau}\right) \tag{32}$$

D_g is the external mass transfer coefficient for the oxidation reaction. σ is the constriction factor, which is a measure of the amount of particle surface area that is normal to the direction of diffusion. ε_g is the void fraction, which accounts for the amount of volume inside a particle that is empty space rather than solid char and is 0.91 for char [12]. τ is the tortuosity, which is a measure of the windiness of a diffusion path. Since σ and τ are difficult to determine, assuming that $\frac{\sigma}{\tau} = 0.2\varepsilon_g$ [13], the expression can be reduced to

$$D_{\text{eff}} = 0.2 D_g \varepsilon_g^2 \tag{33}$$

Since ε_g will vary with conversion, a conversion-averaged diffusion coefficient must be defined as

$$\widehat{D}_{\text{eff}} = D_{\text{g}} \int_0^1 D_{\text{eff}}(X) dX \tag{34}$$

Where

$$X = \frac{\varepsilon_g - \varepsilon_{g,0}}{1 - \varepsilon_{g,0}} \tag{35}$$

Integrating this expression gives

$$\widehat{D}_{eff} = \frac{D_{\text{g}}}{15}\left(\frac{1 - \varepsilon_{g,0}^3}{1 - \varepsilon_{g,0}}\right) \tag{36}$$

STOICHIOMETRIC COEFFICIENT

The stoichiometric coefficient λ is the ratio of carbon to oxygen in the char oxidation reaction. Its value determines the proportion of carbon monoxide and carbon dioxide in the reaction's products.

$$\text{C} + \lambda \text{O}_2 \rightarrow (2 - 2\lambda)\text{CO} + (2\lambda - 1)\text{CO}_2 \tag{37}$$

The lower and upper limits of λ are 0.5 and 1. For λ = 0.5, the only product will be CO, and for λ = 1, the only product will be CO_2. A λ of 0.75 can be assumed for this reaction [14].

THIELE MODULUS

The Thiele modulus ϕ is used to characterize the interaction between diffusion and chemical kinetics in a reacting particle, and is defined as

$$\phi = \frac{\gamma R}{3} \tag{38}$$

The square of the Thiele modulus can be used to compare the rate of internal diffusion to the rate of chemical reactions at the particle surface.

$$\phi^2 = \left(\frac{\gamma R}{3}\right)^2 = \frac{kC_C\lambda}{D_e}\cdot\frac{R^2}{9} = \frac{kC_C\lambda}{D_{\text{eff}}}\cdot\frac{d_p^2}{4\cdot 9} \tag{39}$$

Rearranging this equation gives the timescales of chemical reactions and internal diffusion

$$\phi^2 = \frac{d_p^2}{36D_{\text{eff}}}kC_c\lambda = \frac{\tau_{\text{diff,int}}}{\tau_{\text{rxn}}} \tag{40}$$

where

$$\tau_{\text{rxn}} = (kC_C\lambda)^{-1} \tag{41}$$

$$\tau_{\text{diff,int}} = \frac{d_p^2}{36D_{\text{eff}}} = \frac{(V_p/A_p)^2}{D_{\text{eff}}} \tag{42}$$

A large ϕ indicates an oxidation reaction whose rate is limited by internal mass transfer, while a small ϕ represents a kinetically limited reaction. Rewriting equation **(28)** as a function of ϕ, oxygen concentration inside a particle can be expressed as

$$C_{O_2} = C_s\frac{R}{r}\frac{\sinh(\gamma r)}{\sinh(\gamma R)} = C_s\frac{R}{r}\frac{\sinh\left(3\phi\frac{r}{R}\right)}{\sinh(3\phi)} \tag{43}$$

In Figure 13, oxygen concentration profile is plotted as a function of particle diameter. For $\phi > 3$, oxygen cannot reach the inner radius of the particle and reactions take place over a very small volume fraction of the particle [10].

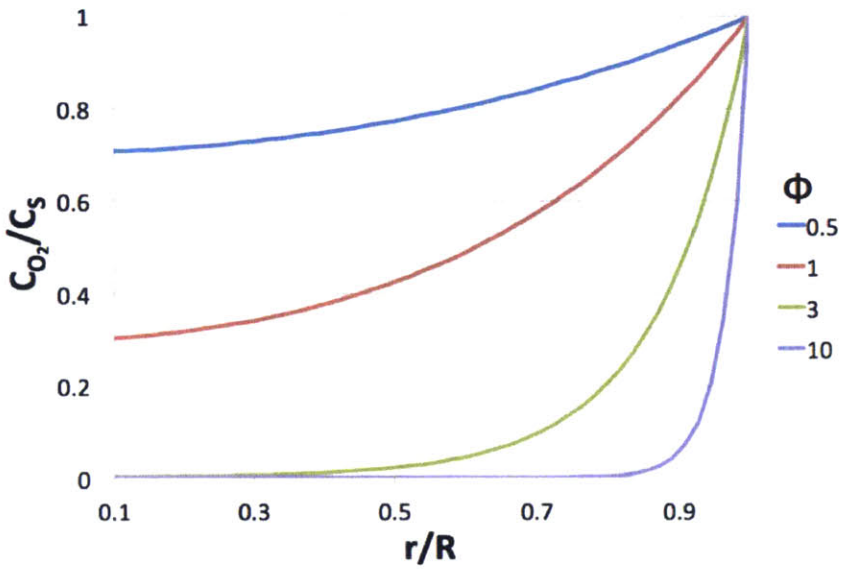

Figure 13: Oxygen concentration profile within a char particle vs. Thiele modulus.

An external Thiele modulus can also be defined to relate the characteristic timescale of external diffusion to that of chemical reactions in the particle. This can be expressed as

$$\phi_{\text{ext}} = \frac{d_p k C_C \lambda}{6 h_m} = \frac{d_p^2}{6 Sh D_g} k C_C \lambda = \frac{\tau_{\text{diff,ext}}}{\tau_{\text{rxn}}} \tag{44}$$

where

$$\tau_{\text{diff,ext}} = \frac{d_p^2}{6 Sh D_g} \tag{45}$$

$$\tau_{\text{rxn}} = (k C_C \lambda)^{-1} \tag{46}$$

EFFECTIVENESS FACTOR

An effectiveness factor can be defined to scale the reaction rate to account for internal diffusion limitations in the overall reaction rate. The effectiveness factor η is a ratio of the actual reaction rate to the maximum reaction rate with no internal diffusion limitations:

$$\eta = \frac{4\pi R^2 J_{\text{particle}}}{\frac{4}{3}\pi R^3 k C_s C_c \lambda} \tag{47}$$

J_{particle} is the mass flux of oxygen at the surface the particle, which can be defined as [11]

$$J_{\text{particle}} = -D_{\text{eff}} \left.\frac{dC_{O_2}}{dr}\right|_{r=R} = D_{\text{eff}} C_s \left(\frac{\gamma}{\tanh(\gamma R)} - \frac{1}{R}\right) \tag{48}$$

The effectiveness factor then becomes

$$\eta = \frac{3D_{\text{eff}}C_s}{RkC_cC_s\lambda}\left(\frac{\gamma}{\tanh(\gamma R)} - \frac{1}{R}\right) = \frac{3}{R\gamma}\left(\frac{1}{\tanh(\gamma R)} - \frac{1}{\gamma R}\right) \tag{49}$$

Rewriting equation (49) in terms of ϕ

$$\eta = \frac{1}{\phi}\left(\frac{1}{\tanh(3\phi)} - \frac{1}{3\phi}\right) \tag{50}$$

$\phi > 3$ is the threshold after which the overall reaction rate can be considered to be limited by internal diffusion, corresponding to zone 2 in Figure 3. Since $\tanh(3\phi) \approx 1$ once $\phi > 3$, the effectiveness factor for internal diffusion limited oxidation will reduce to

$$\eta \sim \frac{1}{\phi}\left(1 - \frac{1}{3\phi}\right) = \frac{1}{\phi} - \frac{1}{3\phi^2} \sim \frac{1}{\phi} = \frac{6}{d_p}\sqrt{\frac{D_{\text{eff}}}{kC_c\lambda}} \tag{51}$$

In Figure 14, effectiveness factor is plotted as a function of Thiele modulus [10].

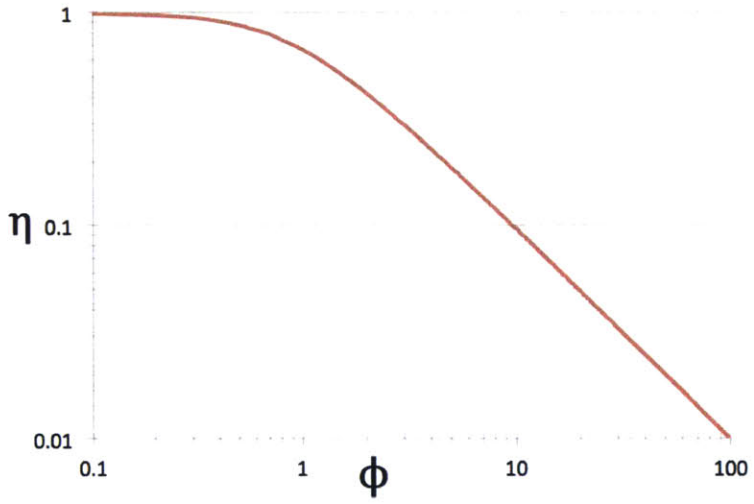

Figure 14: Effectiveness factor η vs. Thiele modulus ϕ for a spherical particle.

An external effectiveness factor can also be defined to relate the actual rate of internal mass transfer to the ideal rate if there were no external mass transfer limitations and therefore no concentration gradient in the particle's boundary layer:

$$\eta_{\text{ext}} = \frac{1}{\eta\phi_{\text{ext}} + 1} = \frac{\text{actual rate}}{\text{rate if } C_s = C_b} \tag{52}$$

2.4.3 Burnout Time for Internal Diffusion-Limited Conditions

The reaction rate for internal diffusion-limited can then be given by

$$r_{\text{eff}}\left[\frac{\text{mol}_{O_2}}{\text{m}^3_{\text{particle}}\cdot\text{s}}\right] = kC_sC_c\lambda\eta \tag{53}$$

Converting from a rate of change in oxygen concentration to a rate of change in carbon mass gives:

$$\frac{dm_C}{dt}\left[\frac{\text{kg}_C}{\text{s}}\right] = \frac{\pi d_p^3}{6}kC_sC_C(MW_C)\eta \tag{54}$$

and subsequently to a rate of change of particle diameter:

$$\frac{dd_p}{dt}\left[\frac{\text{m}}{\text{s}}\right] = \frac{\frac{dm_c}{dt}}{\frac{dm_c}{dd_p}} = \frac{\left(\frac{\pi d_p^3}{6}\right)kC_sC_CMW_C\eta}{\frac{1}{2}\pi d_p^2\rho_C} = \frac{d_pkC_s\eta}{3} \tag{55}$$

For internal diffusion-limited conditions, where $\phi > 3$ and $\eta = \frac{1}{\phi} = \frac{6}{d_p}\sqrt{\frac{D_e}{C_C\lambda}}$, this rate expression reduces to

$$\frac{dd_p}{dt}\left[\frac{\text{m}}{\text{s}}\right] = -\frac{2C_s}{\lambda C_C}\sqrt{kC_C\lambda D_e} \tag{56}$$

The burning rate expression for Zone II will therefore be

$$r_{\text{diff}}\left[\frac{m}{s}\right] = \sqrt{kC_CD_e\lambda} = D_{\text{eff}}\gamma \tag{57}$$

The burnout time under Zone II conditions is then the integral of the above expression [15].

$$t_{\text{b,intMT}} = \frac{d_{\text{char,0}}\,[\text{m}]}{-\frac{dd_p}{dt}\left[\frac{\text{m}}{\text{s}}\right]} = \frac{d_{\text{char,0}}}{\frac{2C_s}{\lambda C_C}\sqrt{kC_CD_{\text{eff}}\lambda}} \tag{58}$$

$$t_{\text{b,intMT}} = \frac{\lambda C_C}{2C_S}\frac{d_{\text{char,0}}}{D_e\gamma} \tag{59}$$

In **Figure 15**, $t_{\text{b,intMT}}$ is plotted as a function of particle diameter at 1 atm and 800°C, and as a function of reactor temperature for a 5 mm particle at 1atm. Both plots use the minimum fluidization velocity for sand, the bed material, and are plotted for three values of λ.

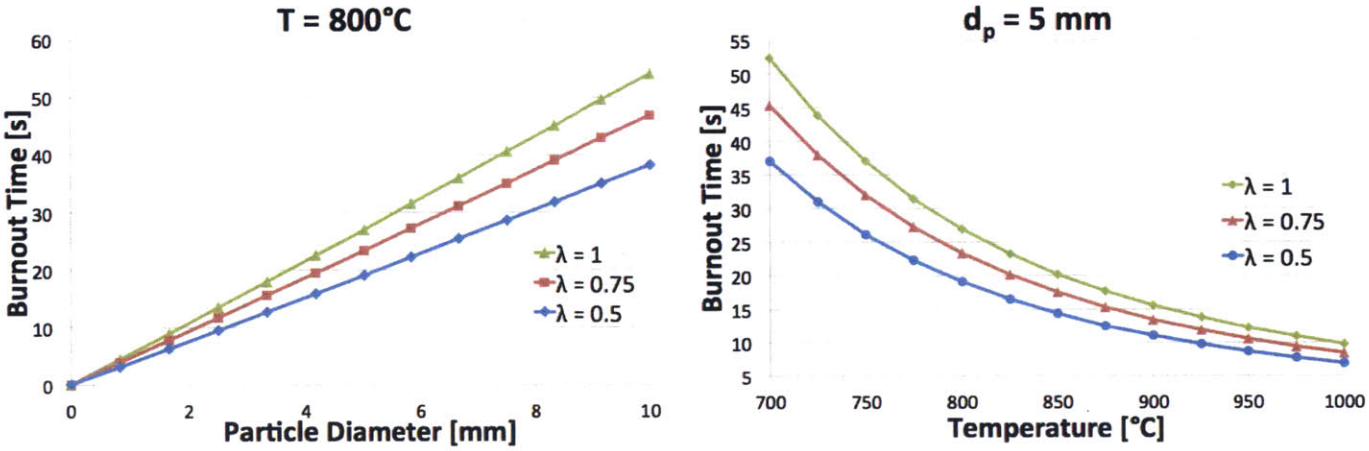

Figure 15: Burnout time under internal diffusion-limited conditions as a function of particle diameter at 1 atm and 800°C, and as a function of temperature at 1 atm for a particle with a 5 mm diameter. Burnout time is shown for three values of lambda, which governs the amounts of CO and CO_2 in the products.

2.5 Overall Char Oxidation Process

In this section, the rates of all three processes will be combined to yield an overall rate expression and burnout time for char oxidation.

2.5.1 Char Oxidation Rate

The mass flux through the particle's boundary layer must equal the mass flux at the particle's surface:

$$J_{\text{particle}}\left[\frac{\text{mol}}{\text{m}^2 \cdot \text{s}}\right] = -D_{\text{eff}}\frac{dC_{O_2}}{dr}\bigg|_{r=R} = h_m(C_s - C_b) \tag{60}$$

Plugging in equation (29) and solving for C_s gives

$$C_s = \frac{h_m C_b}{D_{\text{eff}}\left(\frac{\gamma}{\tanh(\gamma R)} - \frac{1}{R}\right) + h_m} \tag{61}$$

Plugging in the internal effectiveness factor η from equation (49), this can be rewritten as

$$C_s = \frac{C_b}{\eta k C_C \lambda \frac{d_p}{6h_m} + 1} \tag{62}$$

Plugging in the external Thiele modulus from equation (52), this can then be simplified to [12]

$$C_S = \frac{C_b}{\eta\phi_{\text{ext}} + 1} \tag{63}$$

The overall reaction rate from equation (53) is

$$r_{\text{eff}}\left[\frac{\text{mol}_{O_2}}{\text{m}^3_{\text{particle}}\cdot\text{s}}\right] = kC_sC_c\lambda\eta \tag{64}$$

Substituting equation (63) for C_s, the overall reaction rate can be written as

$$r_{\text{eff}}\left[\frac{\text{mol}_{O_2}}{\text{m}^3_{\text{particle}}\cdot\text{s}}\right] = kC_bC_c\lambda\frac{\eta}{\eta\phi_{\text{ext}}+1} \tag{65}$$

Plugging in equation (51) for η and equation (44) for ϕ_{ext}, the rate expression can then be written as

$$r_{\text{eff}}\left[\frac{\text{mol}_{O_2}}{\text{m}^3_{\text{particle}}\cdot\text{s}}\right] = \frac{C_b}{\frac{R}{3h_m}+\frac{1}{D_{\text{eff}}\gamma\eta}} = \frac{C_b}{\tau_{\text{extMT}}+\tau_{\text{intMT,rxn}}} \tag{66}$$

Rewriting equation (66) in terms of η and η_{ext}, the overall rate can also be written as the maximum rate scaled by the effectiveness factors that limit the rate:

$$r_{\text{eff}}\left[\frac{\text{mol}_{O_2}}{\text{m}^3_{\text{particle}}\cdot\text{s}}\right] = kC_bC_c\lambda\eta\eta_{\text{ext}} \tag{67}$$

2.5.2 Char Oxidation Burnout Time

Integrating equation (66) with respect to time and assuming that $\phi > 3$, the overall burnout time will be

$$t_b = \frac{\lambda C_c}{2C_b}\left(\frac{d_{p,0}^2}{2ShD_g}+\frac{d_{p,0}}{D_{\text{eff}}\gamma}\right) \tag{68}$$

From equations (67) and (68), it is apparent that the total burnout time is the sum of the burnout times under externally and internally limited conditions:

$$t_b = t_{\text{b,Zone III}} + t_{\text{b,Zone II}} \tag{69}$$

The processes occurring during char oxidation can therefore be modeled as a series resistance network.

2.6 Conditions under which mass transfer is limiting

For mass transfer limitations to be considered negligible, the timescale for mass transfer must be 10 times less than that of chemical reactions. In terms of the internal and external Thiele modulus, defined in equations (40) and (44):

Internal Mass Transfer:

$$\phi^2 = \frac{d_p^2}{36D_{\text{eff}}} kC_c\lambda = \frac{\tau_{\text{diff,int}}}{\tau_{\text{rxn}}} < \frac{1}{10}$$

External Mass Transfer:

$$\phi_{\text{ext}} = \frac{d_p^2}{6ShD_g} kC_C\lambda = \frac{\tau_{\text{diff,ext}}}{\tau_{\text{rxn}}} < \frac{1}{10} \quad (70)$$

Solving for d_p in this inequality gives the following limitations:

Internal mass transfer limitations can be neglected for

$$d_p < \sqrt{\frac{3.6D_{\text{eff}}}{kC_C\lambda}}$$

External mass transfer limitations can be neglected for

$$d_p < \sqrt{\frac{0.6ShD_g}{kC_C\lambda}} \quad (71)$$

3. Results

3.1 Reaction Rate as a Function of Temperature

In Figures 16-18, reaction rate and internal and external effectiveness factor are plotted as a function of temperature for three particle sizes. Four rates are plotted:

- Reaction rate under purely kinetically-limited conditions:

$$r = kC_C C_B\lambda \quad (72)$$

- Reaction rate under internal diffusion and kinetically-limited conditions

$$r = kC_C C_B\lambda\eta \quad (73)$$

- Reaction rate under external diffusion-limited conditions

$$r = \frac{6h_m C_B}{d_p} \quad (74)$$

- Overall reaction rate

$$r = kC_C C_B\lambda\eta\eta_{\text{ext}} \quad (75)$$

The concentration of carbon in the char particle, C_c, is assumed to be 14,153 molC/m^3, the concentration of carbon in wood chip char [12].

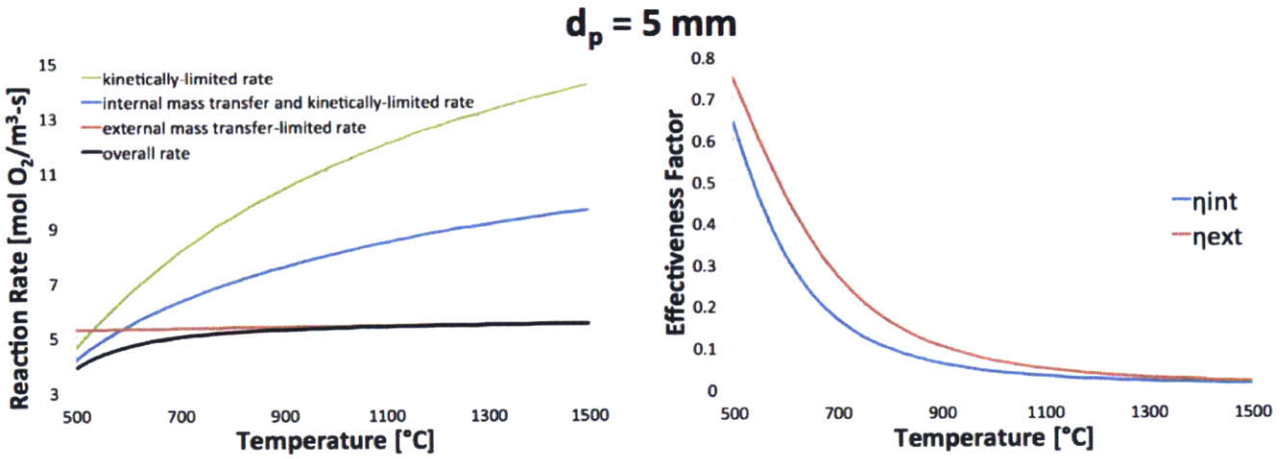

Figure 16: Log of reaction rate under each regime of limitations as a function of temperature for a particle with 5 mm diameter under combustion conditions.

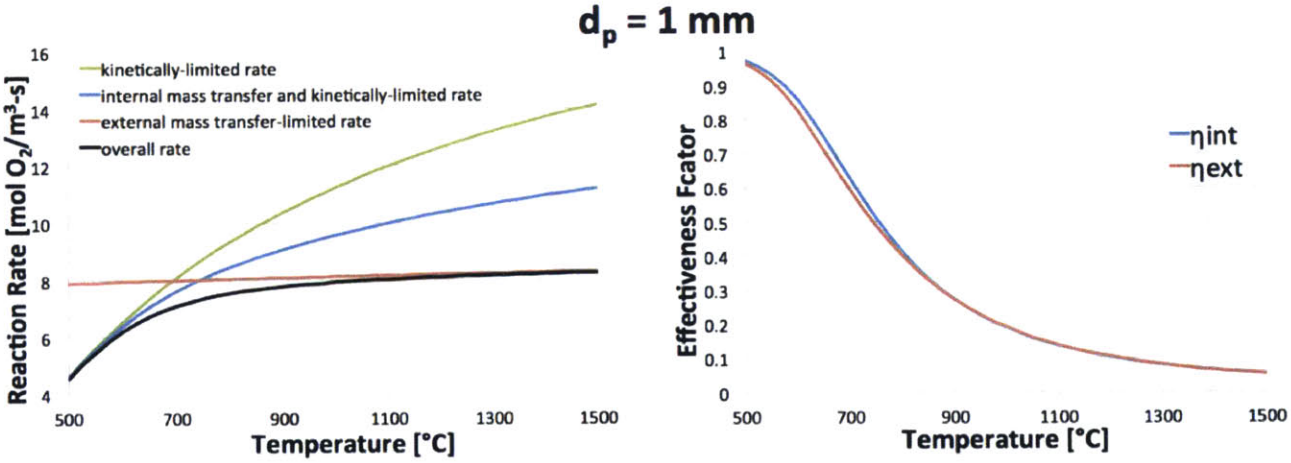

Figure 17: Log of reaction rate under each regime of limitations as a function of temperature for a particle with 1 mm diameter under combustion conditions.

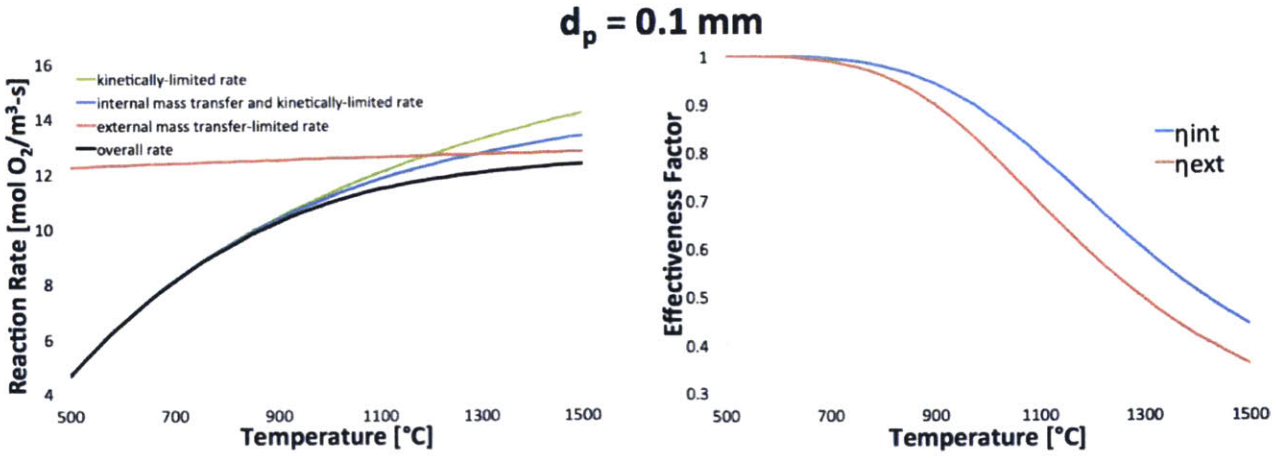

Figure 18: Log of reaction rate under each regime of limitations as a function of temperature for a particle with 0.1 mm diameter under combustion conditions.

A standard size char particle (5 mm) under combustion conditions will be subject primarily to external mass transfer limitations at low temperatures, as the rate of internal diffusion is very fast compared to that of external diffusion. For a smaller particle (1 mm), the overall rate will be limited by internal diffusion at low reactor temperatures, external diffusion at high temperatures, and a combination of both in the middle temperature range. For a very small particle (0.1 mm), the overall rate will be dominated by the rate of internal mass transfer, though the overall rate will be very fast because internal diffusion becomes less limiting over time as the carbonaceous mass of the particle grows smaller. External diffusion is also less limiting at smaller particle diameters since smaller particles will have a smaller boundary layer.

In Figures 19-21, the same four reaction rates are plotted alongside the internal and external effectiveness as a function of particle diameter for three reactor temperatures.

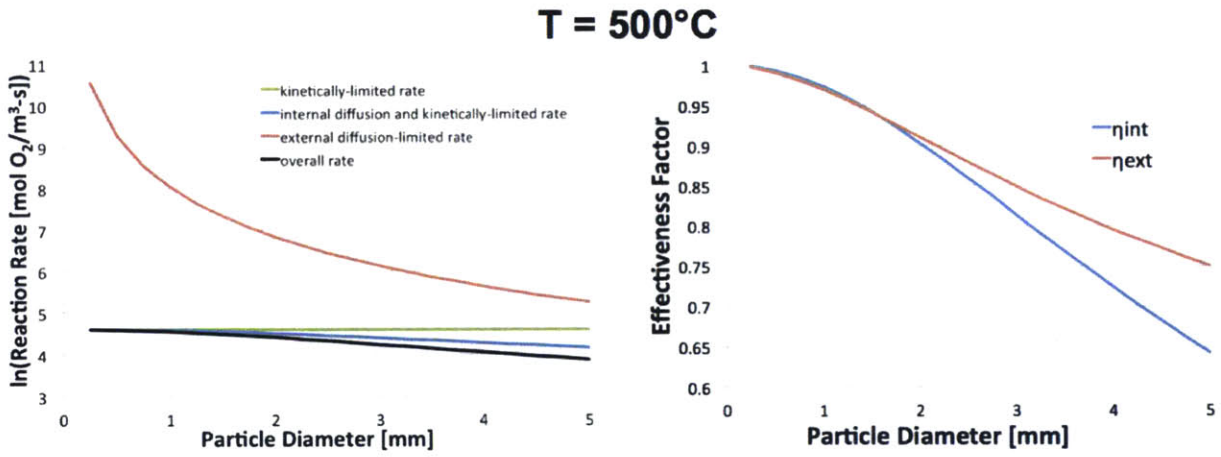

Figure 19: Log of reaction rate and effectiveness factor under each regime of limitations as a function of particle diameter at 500°C under combustion conditions.

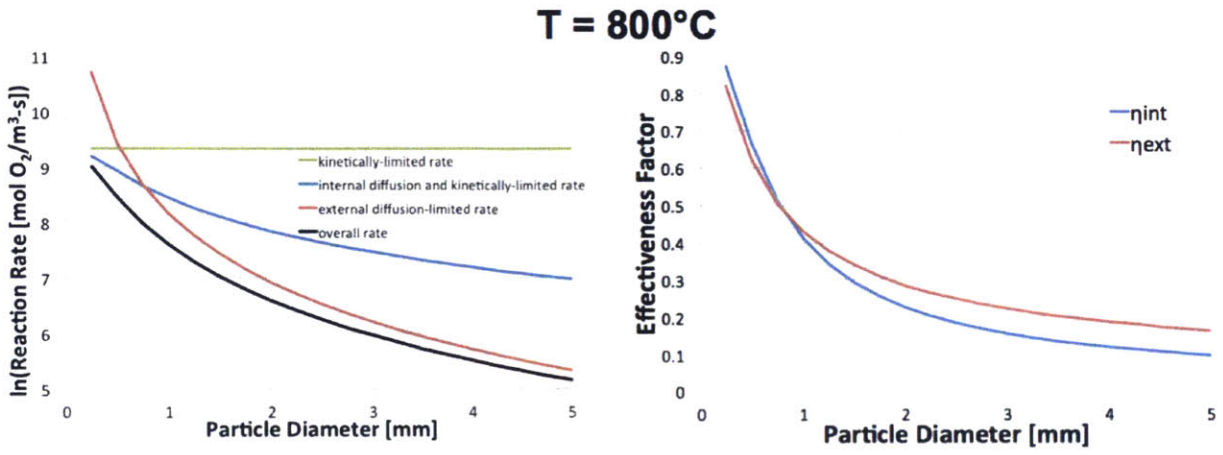

Figure 20: Log of reaction rate and effectiveness factor under each regime of limitations as a function of particle diameter at 800°C under combustion conditions.

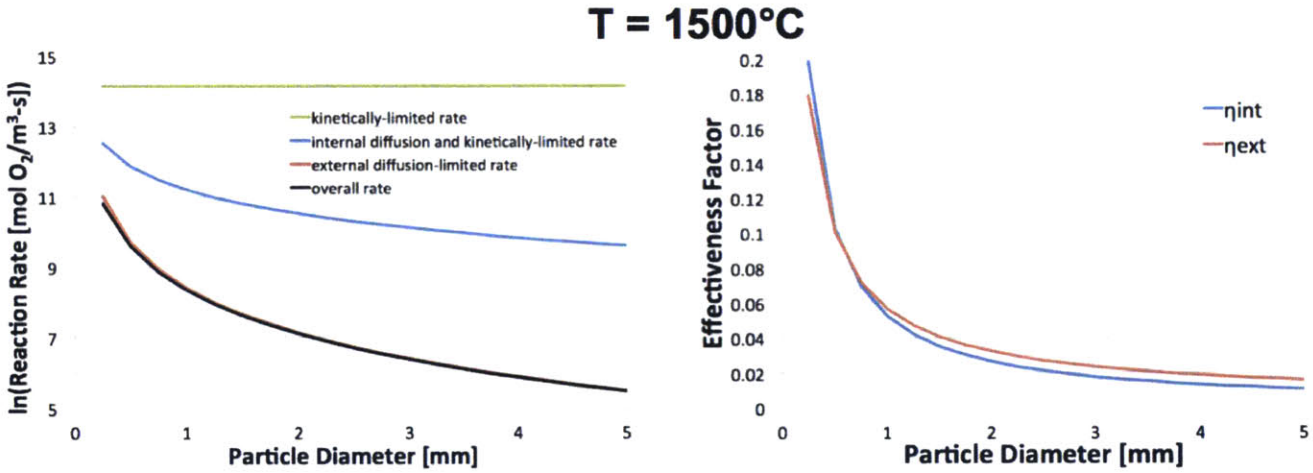

Figure 21: Log of reaction rate and effectiveness factor under each regime of limitations as a function of particle diameter at 1500°C under combustion conditions.

At high temperatures, the overall rate will be entirely dictated by the rate of external mass transfer, while at low temperatures, external mass transfer is very fast, leaving the overall rate ot be limited by the rate of internal diffusion. The rate of chemical reactions becomes very fast and can be neglected when the reaction is at a high temperature. As the reaction proceeds, the char particle will shrink while the reactor is maintained at a constant temperature, and the reaction will approach purely kinetically-limited conditions. It is therefore clear that for most reactor conditions, the oxidation reaction will remain in the mass transfer-limited regime for the majority of the reaction.

3.2 Mass Transfer Limitation Threshold

Figure 22 shows the conditions at or below which mass transfer can be neglected. Each point shows a reactor temperature and particle diameter for which internal or external mass transfer is fast enough to be neglected when modeling overall reaction rate. One can assume that mass transfer can be neglected for all points on or below each line. Internal mass transfer is the more limiting of the two processes. For points below the blue curve, it can be assumed that the reaction is governed by chemical kinetics since it is not subject to any mass transfer limitations. The particle diameters for which mass transfer can be neglected are very small compared to the typical size of a char particle. For example, at 800°C, a typical reactor temperature, char particles must be smaller than 100 μm in diameter in order for mass transfer limitations to be neglected. It is therefore clear that the rate of char oxidation in a FBBG is nearly always limited by mass transfer.

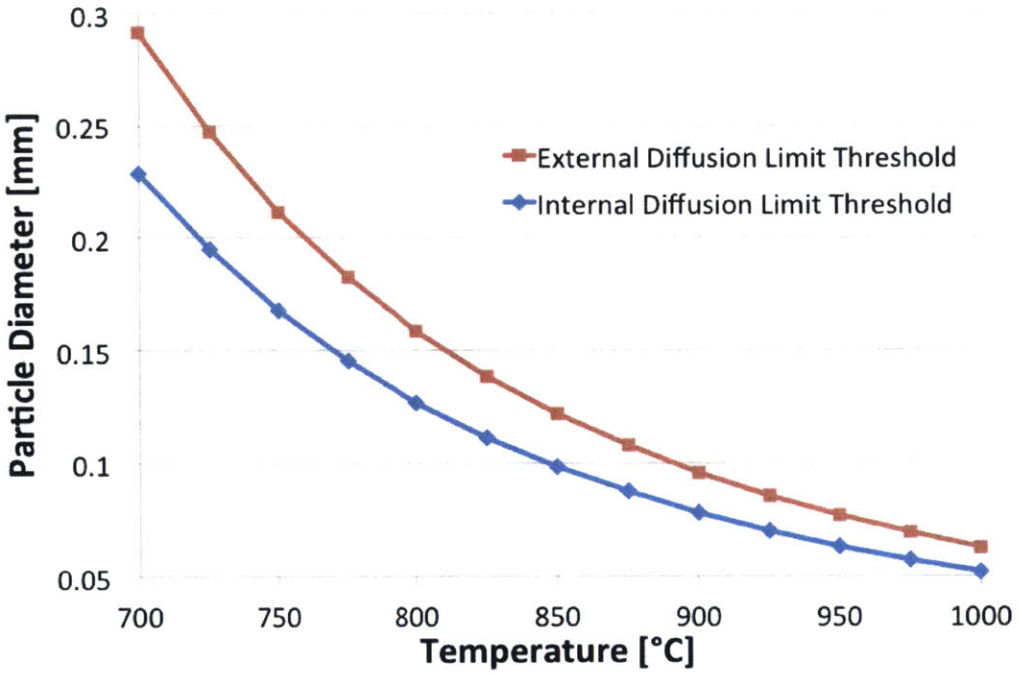

Figure 22: Oxidation conditions (particle diameter and temperature) for which mass transfer can be neglected. Any point on or below one of the curves is not limited by that type of mass transfer.

4. Conclusions

In this study, the timescales of external diffusion, chemical kinetics, and intraparticle diffusion during char conversion in a FBBG were analytically determined for various reactor conditions. These timescales were compared on the basis of reactor temperature and char particle diameter as reactor conditions. This comparison showed which processes limit the overall reaction rate under different reactor conditions and which limitations are small enough to be neglected. This allowed for a set of simplifying assumptions to be made for future reactor modeling. An overall rate expression in terms of internal and external effectiveness factors was formulated which can be applied in reacting CFD simulations. Since all rate expressions scaled linearly with oxygen concentration, the limitations that apply at a given temperature and particle diameter will hold true for all oxygen concentrations.

- For a standard-sized char particle (1-5 mm in diameter) under combustion conditions, the dominant resistance to conversion is external mass transfer.
- For very small particles (~0.1 mm in diameter), external mass transfer limitations can be neglected for temperatures below 1000°C.
- At low reactor temperatures (~500°C), the rate of external mass transfer is very fast can be neglected for all particle sizes.
- At high reactor temperatures (~1500°C), the overall rate is entirely dominated by external mass transfer for all particle sizes, and the rates of kinetics and internal mass transfer can be neglected.

5. References

[1] A. K. Stark, "Multi-Scale Chemistry Modeling of the Thermochemical Conversion of Biomass in a Fluidized Bed Gasifier," Ph.D. Thesis, Massachusetts Institute of Technology, Cambridge, MA, 2015.

[2] S. Gerber, F. Behrendt, and M. Oevermann, "An Eulerian modeling approach of wood gasification in a bubbling fluidized bed reactor using char as bed material," *Fuel*, vol. 89, no. 10, pp. 2903–2917, Oct. 2010.

[3] M. G. Grønli, "A Theoretical and Experimental Study of the Thermal Degradation of Biomass," Ph.D., Norwegian University of Science and Technology, Trondheim, Norway, 1996.

[4] A. N. Hayhurst and M. S. Parmar, "Measurement of the mass transfer coefficient and sherwood number for carbon spheres burning in a bubbling fluidized bed," *Combustion and Flame*, vol. 130, no. 4, pp. 361–375, Sep. 2002.

[5] A. Gómez-Barea, P. Ollero, and B. Leckner, "Mass transport effects during measurements of gas–solid reaction kinetics in a fluidised bed," *Chemical Engineering Science*, vol. 62, no. 5, pp. 1477–1493, Mar. 2007.

[6] G. I. Palchonok, "Palchonok, G.I. et al., 1992. Calculation of true heat and mass transfer coefficients between particles and a fluidized bed. In O. E. Potter & D. J. Nicklin, eds. Fluidization VII. Brisbane, Australia: Engineering Foundation, pp. 913–920.," in *Fluidization*, Brisbane, Australia, 1992, vol. VII, pp. 913–920.

[7] C. Di Blasi, F. Buonanno, and C. Branca, "Reactivities of some biomass chars in air," *Carbon*, vol. 37, pp. 1227–38, 1999.

[8] C. Di Blasi, "Combustion and gasification rates of lignocellulosic chars," *Progress in Energy and Combustion Science*, vol. 35, no. 2, pp. 121–140, Apr. 2009.

[9] T. Kashiwagi and H. Nambu, "Global kinetic constants for thermal oxidative degradation of a cellulosic sample," *Combustion and Flame*, vol. 88, pp. 345–68, 1992.

[10] M. E. Davis and R. J. Davis, *Fundamentals of chemical reaction engineering*. New York, NY: McGraw-Hill Higher Education, 2003.

[11] R. Aris, "On shape factors for irregular particles -- I. The steady-state problem. Diffusion and reaction.," *Chemical Engineering Science*, vol. 6, pp. 262–268, 1957.

[12] F. Scala, R. Chrone, and P. Salatino, "Combustion and Attrition of Biomass Chars in a Fluidized Bed," *Energy Fuels*, vol. 20, no. 1, pp. 91–102, 2006.

[13] R. B. Bates, C. Altantzis, and A. F. Ghoniem, "Bubbling fluidized bed biomass gasification: Modeling of char gasification and attrition kinetics," in *9th U.S. National Combustion Meeting*, Cincinnatti, OH, 2015.

[14] C. Di Blasi, "Modeling wood gasification in a countercurrent fixed-bed reactor," *American Institute of Chemical Engineers*, vol. 50, no. 9, pp. 2306–2319, 2004.

[15] U. Arena, "Some issues in modelling bubbling and circulating fluidized-bed coal combustors," *Powder Technology*, vol. 82, no. 3, pp. 301–316, Mar. 1995.